



# 1 A New Operational Mediterranean Diurnal Optimally Interpolated

## 2 SST Product within the Copernicus Marine Environment

### 3 Monitoring Service

4 Andrea Pisano<sup>1</sup>, Daniele Ciani<sup>1</sup>, Salvatore Marullo<sup>1,2</sup> Rosalia Santoleri<sup>1</sup>, Bruno Buongiorno Nardelli<sup>3</sup>

5 <sup>1</sup>CNR-ISMAR, Via del Fosso del Cavaliere 100, Rome, 00133, Rome, Italy

6 <sup>2</sup>ENEA, Via Enrico Fermi, 45, 00044 Frascati, Italy

7 <sup>3</sup>CNR-ISMAR, Calata Porta di Massa, Napoli, 80133, Italy

8  
9 *Correspondence to:* Andrea Pisano (andrea.pisano@cnr.it)

10 **Abstract.** Within the Copernicus Marine Environment Monitoring Service (CMEMS), a new operational MEDiterranean  
11 Diurnal Optimally Interpolated SST (MED DOISST) product has been developed. This product provides hourly mean maps  
12 (Level-4) of sub-skin SST at 1/16° horizontal resolution over the Mediterranean Sea from January 2019 to present. The product  
13 is built by combining hourly SST data from the Spinning Enhanced Visible and InfraRed Imager (SEVIRI) on board Meteosat  
14 Second Generation and model analyses through optimal interpolation. SEVIRI and model data are respectively used as the  
15 observation source and first-guess. The differences between satellite and model SST are free, or nearly free, of any diurnal  
16 cycle, thus allowing them to be interpolated in space and time using satellite data acquired at different times of the day. The  
17 accuracy of the MED DOISST product is assessed here by comparison against surface drifting buoy measurements, covering  
18 the years 2019 and 2020. The diurnal cycle reconstructed from DOISST is in good agreement with the one observed by  
19 independent drifter data, with a mean bias of  $0.041 \pm 0.001$  K and root-mean-square difference (RMSD) of  $0.412 \pm 0.001$  K.  
20 The new SST product is more accurate than the input model during the central warming hours, when the model, on average,  
21 underestimates drifter SST by one tenth of degree. The MED DOISST product is also able to reproduce accurately the extreme  
22 diurnal warming events frequently observed in the Mediterranean Sea, which may reach amplitudes larger than 5 K during the  
23 warm season. This product can contribute to improve the prediction capability of numerical weather forecast systems (e.g.,  
24 through improved forcing/assimilation), as well as the monitoring of surface heat budget estimates and temperature extremes  
25 which can have significant impacts on the marine ecosystem.

26  
27 The full MED DOISST product (released on 04 May 2021) is available upon free registration at  
28 [https://doi.org/10.25423/CMCC/SST\\_MED\\_PHY\\_SUBSKIN\\_L4\\_NRT\\_010\\_036](https://doi.org/10.25423/CMCC/SST_MED_PHY_SUBSKIN_L4_NRT_010_036) (Pisano et al., 2021). The reduced subset  
29 used here for validation and review purposes is openly available at <https://doi.org/10.5281/zenodo.5807729> (Pisano, 2021).



30

## 31 **1 Introduction**

32 In the last decades, the development of accurate satellite-based Sea Surface Temperature (SST) products required an increasing  
33 effort to meet an ever-growing request from scientific, operational and emerging policy needs. Indeed, infrared and/or  
34 microwave satellite radiometers allow a systematic and synoptic mapping of the ocean surface temperature (under clear-sky  
35 conditions for the infrared and in the absence of rain for the microwave bands) with spatial resolutions from one to few  
36 kilometers and temporal sampling from hourly to daily (Minnett et al., 2019). This almost continuous coverage represents a  
37 unique characteristic of satellite thermal data, which is clearly not achievable with the use of in situ measurements alone.  
38 Indeed, though in situ sensors reach significantly higher accuracy than satellite sensors, with uncertainties that can reach  $O(10^{-2}^{\circ}\text{C})$ ,  
39 they provide pointwise seawater temperature measurements, generally characterized by a poor and non-uniform sampling  
40 of the ocean surface.

41 There is a huge variety of satellite-based SST datasets, characterized by different nominal resolutions as well as temporal and  
42 spatial (global or regional) coverage, and based on different processing algorithms and satellite sensors, but designed to provide  
43 highly accurate SST estimates (Yang et al., 2021). Operational datasets are typically distributed in near real time (NRT),  
44 delayed-mode or as reprocessed datasets, and may include different processing levels, from single satellite passes processed  
45 to provide valid SST values in the original observation geometry, the so-called Level-2 (L2), to images remapped onto a regular  
46 grid, also known as Level-3 (L3), up to the spatially complete Level-4 (L4), interpolated over fixed regular grids. These latter  
47 are required by several applications since the lower levels are typically affected by several data voids (due to clouds, rain, land,  
48 sea-ice, or other environmental factors depending on the type of sensors). The timely availability of SST data, ranging from a  
49 few hours to a few days before real time, allows their use as boundary condition and/or assimilation in meteorological and  
50 ocean forecasting systems (Waters et al., 2015), to improve the retrieval of ocean surface currents (Bowen et al., 2002; Rio  
51 and Santoleri 2018), and monitor some weather extreme events, such as marine heatwaves (Oliver et al., 2021). The  
52 reprocessing of long-term SST data records, typically covering the satellite era (1981-present), aims to provide more stable  
53 and consistent datasets, complementing the NRT production, to be used to investigate climate variability and monitor changes  
54 from interannual to multi-decadal timescales (Deser et al., 2010), including e.g. SST trends' estimates (Good et al., 2007;  
55 Pisano et al., 2020). The Copernicus Marine Environment Monitoring Service (CMEMS) is one of the main examples of how  
56 satellite observations, including not only SST but a wide range of surface variables (e.g., sea surface salinity, sea surface  
57 height, ocean color, winds and waves), are exploited to derive and disseminate high-level products (Le Traon et al., 2019),  
58 namely L4 data in order to be directly usable for downstream applications.

59 The majority of the existing L4 SST datasets are provided as daily, weekly or monthly averaged fields (see e.g. Fiedler et al.,  
60 2019; Yang et al., 2021). Examples of well-known state-of-the-art SST daily datasets include the Global Ocean Sea Surface



61 Temperature and Sea Ice (OSTIA) dataset (Good et al., 2020), the European Space Agency (ESA) Climate Change Initiative  
62 (CCI), the Copernicus Climate Change Service (C3S) Reprocessed Sea Surface Temperature Analyses (Merchant et al., 2019),  
63 and the NOAA Daily Optimally Interpolated SST (OISST) v2.1 dataset, previously known/referred to as Reynolds SST  
64 analysis (Huang et al., 2021). Though a daily resolution is generally sufficient to meet the requirements of many of the  
65 oceanographic applications, it does not resolve the SST diurnal cycle, the typical day-night SST oscillation mainly driven by  
66 solar heating. Within the oceanic thermal skin layer (few  $\mu\text{m}$  to 1 mm), SST is typically subject to a large potential diurnal  
67 cycle (especially under low wind speed and strong solar heating conditions) reaching amplitudes up to 3 K in the world oceans  
68 (Gentemann et al., 2008; Gentemann and Minnett, 2008).

69 The SST diurnal cycle has several implications on mixed layer dynamics, air-sea interaction and the modulation of the lower  
70 atmosphere dynamics. The most direct consequence of the SST diurnal amplitude variability is certainly on air-sea fluxes.  
71 Clayson and Bogdanoff (2013) estimated that the diurnal SST cycle contributes with slightly less than that  $5 \text{ W m}^{-2}$  to the global  
72 ocean-atmosphere heat budget with peaks of about  $10 \text{ W m}^{-2}$  in the Tropics. The inclusion of a realistic diurnal SST cycle in  
73 atmospheric numerical simulation also has a non-negligible impact on cloud dynamics. Chen and Houze (1997) have shown  
74 that in the Tropical Warm Pool, where extreme localized warming events occur, the diurnal warming can contribute to  
75 modulate the evolution of convective clouds and, more in general, can impact the ocean-atmosphere coupling in numerical  
76 models, producing a more realistic spatial pattern of warming and precipitation (Bernie et al., 2008). Overall, the diurnal cycle  
77 of SST is generally underestimated in current ocean models and the assimilation of SST at high temporal frequency has the  
78 potential to improve sea surface variability and mixed layer accuracy (Storto and Oddo, 2019).

79 In principle, the best opportunity to measure the diurnal cycle comes from infrared radiometers on board geostationary  
80 satellites. Their observations are sufficiently accurate and frequent to resolve the diurnal signal variability whenever cloud  
81 cover is not too persistent. An example is provided by the Spinning Enhanced Visible Infra-Red Imager (SEVIRI) onboard the  
82 Meteosat Second Generation (MSG) geostationary satellite covers. The operational retrieval of SST from MSG/SEVIRI  
83 (managed by the European Organization for the Exploitation of Meteorological Satellites, EUMETSAT, Ocean and Sea-Ice  
84 Facility, OSI-SAF) produces L3C hourly sub-skin SST products by aggregating 15 minutes (MSG/SEVIRI) observations  
85 within 1 hour. The sub-skin SST is the temperature at the base of the conductive laminar sub-layer of the ocean surface, as  
86 defined by the Group of High Resolution SST (GHRSSST, see e.g. Minnett et al., 2019). In practice, this is the temperature at  
87  $\sim 1$  mm depth, and thus particularly sensitive to diurnal warming.

88 For the global ocean, the Operational Sea surface Temperature and sea Ice Analysis (OSTIA) diurnal product (While et al.,  
89 2017) provides daily gap-free maps of hourly mean skin SST at  $0.25^\circ \times 0.25^\circ$  horizontal nominal resolution, using in situ and  
90 satellite data from infrared radiometers. The skin SST is the temperature within the conductive diffusion-dominated sub-layer  
91 at a depth of  $\sim 10\text{-}20 \mu\text{m}$  (as defined by GHRSSST, Minnett et al., 2019). This system produces a skin SST by combining the



92 OSTIA foundation SST analysis (Good et al., 2020) with a diurnal warm-layer temperature difference and a cool skin  
93 temperature difference derived from numerical models.

94 At regional scale, a method to reconstruct the hourly SST field over the Mediterranean Sea from SEVIRI data has been  
95 proposed by Marullo et al. (2014, 2016). The reconstruction is based on a blending of satellite observations and numerical  
96 model analyses (used as first-guess) using optimal interpolation. Though model analyses by definition also assimilate  
97 observations, which could thus in principle include hourly SEVIRI data, in the present configuration they are not able to deal  
98 with such frequent updates (see section 2.2), and the approach presented here represents an effective way to improve the  
99 reconstruction of SST daily cycle from high-repetition satellite measurements. Previous works demonstrated the capability of  
100 SEVIRI to resolve the SST diurnal variability and to reconstruct accurate L4 SST hourly fields over the Mediterranean Sea, a  
101 basin that exhibits large diurnal SST variations (Buongiorno Nardelli et al., 2005; Minnett et al., 2019) that can easily exceed  
102 extreme values ( $\sim 5$  K) as observed in the Tropical Pacific (Chen and Houze 1997), in the Atlantic Ocean and other marginal  
103 seas (Gentemann et al., 2008; Merchant et al., 2008). The aim of this paper is to describe the operational implementation of a  
104 diurnal optimally interpolated SST (DOISST) product for the Mediterranean Sea (MED) at  $1/16^\circ$  horizontal resolution,  
105 building on the algorithm by Marullo et al. (2014, 2016). The assessment of the MED DOISST product covers two complete  
106 years (2019-2020), thus extending previous similar validations (Marullo et al., 2016).

107

## 108 **2 The data**

### 109 **2.1 Satellite data**

110 Input satellite SST is derived from the SEVIRI sensor onboard the Meteosat Second Generation (Meteosat-11) satellite.  
111 SEVIRI has a repeat cycle of 15 minutes over the 60S-60N and 60W-60E domain: Atlantic Ocean, European Seas and western  
112 Indian Ocean. The retrieval of SST from Meteosat-11/SEVIRI is managed by EUMETSAT OSI-SAF, which provides sub-  
113 skin SST data as aggregated (L3C) hourly products remapped onto a  $0.05^\circ$  regular grid. Hourly products result from  
114 compositing the best SST measurements available in one hour and are made available in near real time with a timeliness of 3  
115 hours (see the OSI-SAF product user manual, <https://osi-saf.eumetsat.int/products/osi-206>). File format follows the Data  
116 Specification (GDS) version 2 from the Group for High Resolution Sea Surface Temperatures (GHRSSST, [https://podaac-  
117 tools.jpl.nasa.gov/drive/files/OceanTemperature/ghrsst/docs/GDS20r5.pdf](https://podaac-tools.jpl.nasa.gov/drive/files/OceanTemperature/ghrsst/docs/GDS20r5.pdf)). The computation of SST in day and night  
118 conditions is based on a nonlinear split window algorithm whose coefficients are determined from brightness temperature  
119 simulations on a radiosonde profile database, with an offset coefficient corrected relative to buoy measurements. A correction  
120 term derived from simulated brightness temperatures with an atmospheric radiative transfer model is then applied to the  
121 multispectral derived SST (OSI-SAF PUM, [https://osi-saf.eumetsat.int/lml/doc/osisaf\\_cdop3\\_ss1\\_pum\\_geo\\_sst.pdf](https://osi-saf.eumetsat.int/lml/doc/osisaf_cdop3_ss1_pum_geo_sst.pdf)). L3C



122 data are provided with additional information, including quality level and cloud flags. Such quality flags are provided at pixel  
123 level, ranging over a scale of five levels with increasing reliability: 1 (=“cloudy”), 2 (=“bad”), 3 (=“acceptable”), 4 (=“good”)  
124 to 5 (=“excellent”).

125 The accuracy of Meteosat-11 SST data has been assessed through comparison with co-located drifting buoys, for day and  
126 night data separately covering the period from February to June 2018 (see the OSI-SAF scientific validation report, [https://osi-  
127 saf.eumetsat.int/lml/doc/osisaf\\_cdop2\\_ssl\\_geo\\_sst\\_val\\_rep.pdf](https://osi-saf.eumetsat.int/lml/doc/osisaf_cdop2_ssl_geo_sst_val_rep.pdf)). The mean bias and standard deviation (derived from the  
128 differences between SEVIRI SSTs and drifter measurements over a matchup database) during nighttime have been quantified  
129 in -0.1 K and 0.53 K, respectively. During daytime, the bias remains practically unchanged (-0.09 K) and the standard deviation  
130 slightly higher (0.56 K). These statistics were derived by selecting SEVIRI SST with quality flags  $\geq 3$ , and it is shown that  
131 the quality of SST improves when choosing higher quality levels.

132 For our purposes, we selected L3C SST data with quality flag  $\geq 3$ , as also indicated/suggested in the OSI-SAF scientific  
133 validation report.

## 134 **2.2 Model data**

135 The model output fields of surface temperature are derived from the CMEMS Mediterranean Sea Physical Analysis and  
136 Forecasting product, and identified as MEDSEA\_ANALYSIS\_FORECAST\_PHY\_006\_013  
137 ([https://resources.marine.copernicus.eu/product-  
138 detail/MEDSEA\\_ANALYSISFORECAST\\_PHY\\_006\\_013/INFORMATION](https://resources.marine.copernicus.eu/product-detail/MEDSEA_ANALYSISFORECAST_PHY_006_013/INFORMATION);  
139 [https://doi.org/10.25423/CMCC/MEDSEA\\_ANALYSISFORECAST\\_PHY\\_006\\_013\\_EAS6](https://doi.org/10.25423/CMCC/MEDSEA_ANALYSISFORECAST_PHY_006_013_EAS6); last access: 03 November 2021;  
140 Clementi et al., 2021), and routinely produced by the CMEMS Mediterranean Monitoring and Forecasting Center (Med-MFC).  
141 The modelling system is based on the Mediterranean Forecasting System, MFS (Pinaridi et al., 2003), a coupled hydrodynamic-  
142 wave model implemented over the Mediterranean basin, extended into the Atlantic Sea in order to better resolve the exchanges  
143 with the Atlantic Ocean at the Strait of Gibraltar, with a horizontal grid resolution of  $1/24^\circ$  ( $\sim 4$  km) and 141 unevenly spaced  
144 vertical levels (Clementi et al., 2017). The Ocean General Circulation Model is based on the Nucleus for European Modelling  
145 of the Ocean (NEMO v3.6) (Oddo et al., 2014, 2009), while the wave component is provided by Wave Watch-III. The model  
146 solutions are corrected by a variational data assimilation scheme (3DVAR) of temperature and salinity vertical profiles and  
147 along track satellite sea level anomaly observations (Dobricic and Pinaridi 2008). The CMEMS Mediterranean SST L4 product  
148 (CMEMS product reference: SST\_MED\_SST\_L4\_NRT\_OBSERVATIONS\_010\_004,  
149 [https://resources.marine.copernicus.eu/product-  
150 detail/SST\\_MED\\_SST\\_L4\\_NRT\\_OBSERVATIONS\\_010\\_004/INFORMATION](https://resources.marine.copernicus.eu/product-detail/SST_MED_SST_L4_NRT_OBSERVATIONS_010_004/INFORMATION); last access: 03 November 2021) is used for  
151 the correction of surface heat fluxes with the relaxation constant of  $110 \text{ Wm}^{-2}\text{K}^{-1}$  centered at midnight since the product  
152 provides foundation SST ( $\sim$ SST at midnight).



153 The Med-MFC product is produced with two different cycles: a daily cycle for the production of forecasts (i.e., ten-days  
154 forecast on a daily basis), and a weekly cycle for the production of analyses. For our purposes, only hourly mean fields of sea  
155 surface temperature, which correspond to the first vertical level of the model centered at ~1 m from the surface, are selected.

## 156 **2.3 In situ data**

157 In situ data have been used for validation purposes (Section 4). Specifically, only surface drifting buoys have been used due  
158 to both their closeness to the sea surface (typically ~20 cm from the surface; Reverdin et al., 2010) and to their much larger  
159 number compared to other in situ instruments, which allows a more consistent and homogeneous temporal and spatial coverage.

160 Drifter data have been obtained from the CMEMS IN SITU (INS) TAC (identified as  
161 INSITU\_MED\_NRT\_OBSERVATIONS\_013\_035, [https://resources.marine.copernicus.eu/product-](https://resources.marine.copernicus.eu/product-detail/INSITU_MED_NRT_OBSERVATIONS_013_035/INFORMATION)  
162 [detail/INSITU\\_MED\\_NRT\\_OBSERVATIONS\\_013\\_035/INFORMATION](https://resources.marine.copernicus.eu/product-detail/INSITU_MED_NRT_OBSERVATIONS_013_035/INFORMATION); and  
163 INSITU\_IBI\_NRT\_OBSERVATIONS\_013\_033, [https://resources.marine.copernicus.eu/product-](https://resources.marine.copernicus.eu/product-detail/INSITU_IBI_NRT_OBSERVATIONS_013_033/INFORMATION)  
164 [detail/INSITU\\_IBI\\_NRT\\_OBSERVATIONS\\_013\\_033/INFORMATION](https://resources.marine.copernicus.eu/product-detail/INSITU_IBI_NRT_OBSERVATIONS_013_033/INFORMATION); last access: 03 November 2021), which collects  
165 and distributes a variety of physical and biogeochemical seawater measurements, provided with the same homogeneous file  
166 format. Each in situ measurement, including drifters, undergoes automated quality controls before its distribution. The quality  
167 of the data is expressed by control flags indexed from 0 to 9, with the value of 1 indicating best quality. Drifter data have been  
168 used to compile an hourly matchup database of co-located (in space and time) diurnal optimally interpolated SST (DOISST)  
169 values and model outputs (Section 4.1), and validation statistics are based on the comparison between DOISST, model SST  
170 and drifting buoy measurements over the matchup database (Section 4.2).

## 171 **3 The Mediterranean diurnal optimally interpolated SST product**

### 172 **3.1 Product overview**

173 The Mediterranean diurnal optimally interpolated SST (hereafter referred to as MED DOISST) operational product consists  
174 of hourly mean gap-free (L4) satellite-based estimates of the sub-skin SST over the Mediterranean Sea (plus the adjacent  
175 Eastern Atlantic box, see Section 2.2) at 0.0625° x 0.0625° grid resolution, from 1st January 2019 to near real time.  
176 Specifically, the product is updated daily and provides 24 hourly mean data of the previous day, centered at 00:00, 01:00,  
177 02:00,..., 23:00 UTC. The MED DOISST product is published on the CMEMS on line catalogue and identified as  
178 SST\_MED\_PHY\_SUBSKIN\_L4\_NRT\_010\_036 (CMEMS product reference) and cmems\_obs-sst\_med\_phy-  
179 sst\_nrt\_diurnal-oi-0.0625deg\_PT1H-m (CMEMS dataset reference). A synthesis of the product characteristics is shown Table  
180 1.

181

---

CMEMS Product ID: SST\_MED\_PHY\_SUBSKIN\_L4\_NRT\_010\_036



<b>CMEMS Dataset ID:</b> cmems_obs-sst_med_phy-sst_nrt_diurnal-oi-0.0625deg_PT1H-m	
<b>General description</b>	<p>The CMEMS Mediterranean diurnal product provides near-real-time, hourly mean, gap-free (L4) sub-skin SST fields over the Mediterranean Sea and the adjacent Atlantic box over a 0.0625°x0.0625° regular grid, covering the period from 2019 to present (one day before real time). This product is built from optimal interpolating the Level-3C (merged single-sensor, L3C) SEVIRI data as observations and the CMEMS Mediterranean model analyses as first-guess.</p> <div style="text-align: center;"> </div>
<b>Horizontal resolution</b>	0.0625° x 0.0625° (1/16°) degrees [871x253]
<b>Temporal resolution</b>	Hourly
<b>Spatial coverage</b>	Mediterranean Sea + adjacent North Atlantic box (W=-18.1250, E=36.2500, S=30.2500, N=46.0000)
<b>Temporal coverage</b>	2019/01/01 – near real time (-14H)
<b>Variables</b>	Sub-skin SST (K) Analysis Error (%)
<b>Format</b>	NetCDF – CF-1.4 convention compliant
<b>DOI</b>	<a href="https://doi.org/10.25423/CMCC/SST_MED_PHY_SUBSKIN_L4_NRT_010_036">https://doi.org/10.25423/CMCC/SST_MED_PHY_SUBSKIN_L4_NRT_010_036</a>
<b>Comments</b>	Eventual updates of this product will be described in the corresponding Product User Manual (PUM) and Quality Information Document (QUID) available on the CMEMS on line catalogue.

182

183 **Table 1.** The CMEMS MED DOISST product description synthesis.

184

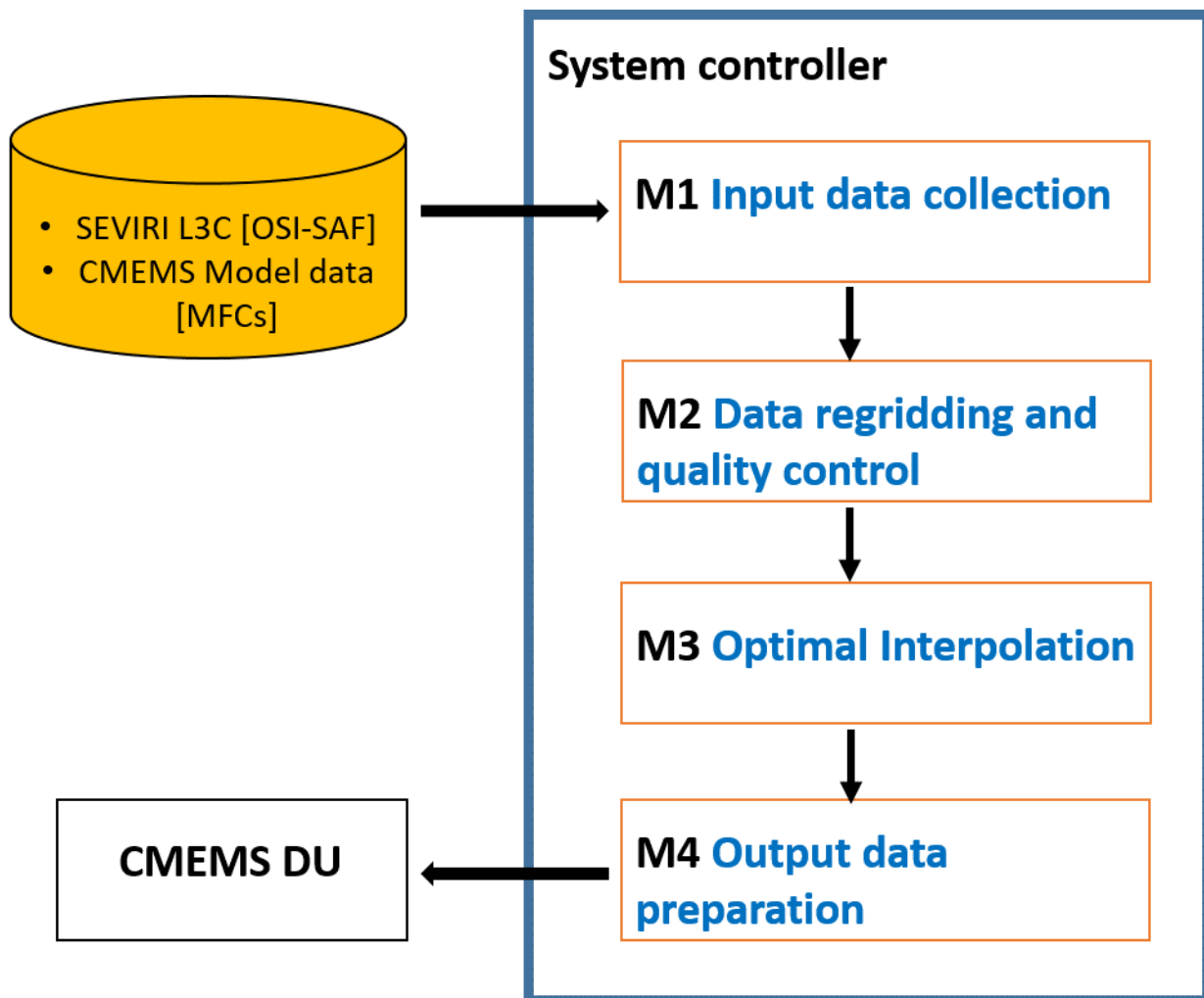
### 185 3.2 Processing chain

186 The system implements the DOISST scheme developed by Marullo et al. (2014). The system ingests merged single-sensor  
 187 (L3C) SEVIRI data as the observation source, and the CMEMS Mediterranean Sea model outputs as first-guess. It has been  
 188 shown that the diurnal signal in the hourly anomaly SST field (satellite-model) is reduced by about one order of magnitude  
 189 with respect to the full signal, thus allowing to interpolate SST anomalies using satellite data acquired at different times of the



190 day (Marullo et al., 2014). Several trials over a large variety of environmental conditions have shown that the temporal window  
191 to be used for the selection of input observations is  $\pm 24$  hours.

192 The data sub-sampling strategy, inversion technique and numerical implementation of the optimal interpolation  
193 scheme are based on the CMEMS NRT MED SST processing chain (Buongiorno Nardelli et al., 2013), which provides daily  
194 mean fields of foundation SST over the Mediterranean Sea (CMEMS product reference:  
195 SST\_MED\_SST\_L4\_NRT\_OBSERVATIONS\_010\_004, [https://resources.marine.copernicus.eu/product-  
196 detail/SST\\_MED\\_SST\\_L4\\_NRT\\_OBSERVATIONS\\_010\\_004/INFORMATION](https://resources.marine.copernicus.eu/product-detail/SST_MED_SST_L4_NRT_OBSERVATIONS_010_004/INFORMATION); last access: 03 November 2021). Here, the  
197 diurnal SST chain is organized in three main modules (Fig. 1).



198  
199 **Figure 1.** Schematic diagram of the processing chain used for the MED DOISST SST product.





200  
201 Module M1 manages the external interfaces to get both upstream L3C SST and model data: hourly mean L3C sub-skin SST  
202 data at 0.05° grid resolution are downloaded from OSI-SAF; hourly seawater potential temperatures at 1.0182 meter are  
203 obtained from the CMEMS Mediterranean Sea model outputs.

204 Module M2 extracts and regrids (through bilinear interpolation) L3C data and model outputs over the CMEMS Mediterranean  
205 Sea geographical area. A selection over SEVIRI is performed by flagging the pixels with quality flag < 3.

206 Module M3 performs a space-time optimal interpolation (OI) algorithm. L4 data are obtained as a linear combination of the  
207 SST anomalies, weighted directly with their correlation to the interpolation point and inversely with their cross-correlation and  
208 error. Correlations are typically expressed through analytical functions with predefined spatial and temporal de-correlation  
209 lengths. Here, the covariance function  $f(r, \Delta t)$  is the one defined in Marullo et al. (2014), and given as the product of a spatial  
210 and temporal component:

$$211 \quad f(r, \Delta t) = f(r) * f(\Delta t) = [a * \exp(-r/R) + (1.-a)/(1.+r)c] * \exp(-(\Delta t/T)d)$$

212  
213

214 where  $r$  is the distance (in km) between the observation and the interpolation point;  $\Delta t$  is the temporal difference (in hours)  
215 between the observation and the interpolation point;  $R = 200$  km is the decorrelation spatial length;  $T = 36$  h is the decorrelation  
216 time length; the other parameters are set as follows:  $a = 0.70$ ,  $c = 0.26$ ,  $d = 0.4$ . All these parameters have been deduced from  
217 a statistical analysis of the satellite SST data.

218 The input data are selected only within a limited sub-domain (within a given space-time interval), with a temporal window of  
219  $\pm 24$  h (Marullo et al., 2014) and a spatial search radius of about 700 km (Buongiorno Nardelli et al., 2013). A check to avoid  
220 data propagation across land is performed between each pixel within the sub-domain and the given interpolation point  
221 (eventually discarded if there are land pixels between the straight line connecting the two points).

222 The interpolation error (analysis\_error field in the L4 file, Table 1) is obtained from the formal definition of the error variance  
223 derived from optimal interpolation theory (e.g., Bretherton et al., 1976). This error ranges between [0,100%], meaning that all  
224 observations are used (no first-guess data are used) when the error is zero, while only first-guess data are used (i.e no  
225 observations available) when the error is 100%.

226 The optimal interpolation algorithm is synthetized as follows:

- 227 • Hourly SEVIRI and model SSTs in a space/time window of 700 km/  $\pm 24$  h around the interpolation position/time are  
228 ingested;
- 229 • SEVIRI data with quality flag  $\geq 3$  are retained;



- 230 • Regridding over the Mediterranean Sea;
- 231 • Hourly model SSTs are subtracted from valid SSTs producing SST anomalies;
- 232 • SST anomalies are used as data input for the optimal interpolation analysis;
- 233 • Optimal interpolation is run using the covariance function defined above;
- 234 • The model SST is added to the optimally interpolated output again.

235

236 The only difference with the original method is that all the input observations are interpolated, while in Marullo et al. (2014)  
237 valid SST observations are left unchanged (not interpolated).

## 238 **4 Validation of diurnal product**

### 239 **4.1 Validation framework**

240 The accuracy of the MED DOISST product has been assessed through comparison with independent co-located (in space and  
241 time) surface drifting buoy data (matchups). The validation framework is based on the compilation of a matchup database  
242 between DOISST and drifters measurements covering the full years 2019 and 2020. The large number of drifters provides a  
243 rather homogeneous and continuous spatial and temporal coverage over the whole period (Fig. 2) allowing a robust statistical  
244 approach.

245 Firstly, a pre-selection of high-quality drifter data is performed, retaining only temperatures with quality flag equal to 1 (good)  
246 or 2 (probably good) (see section 2.3). Then, the validation is carried out on hourly basis, building a matchup database by  
247 collecting the closest (in space) SST grid point to the in situ measurement within a symmetric temporal window of 30 minutes  
248 with respect to the beginning of each hour. A final quality control iteratively identifies drifter temperatures for which the  
249 module of the difference between satellite and drifter temperature exceeds  $n$ -times the standard deviation  $\sigma$  of the distribution  
250 of all these differences ( $\delta$ ). At each step of decreasing  $n$ , data that falls out of the interval  $I = [mean(\delta) - n \cdot \sigma, mean(\delta) +$   
251  $n \cdot \sigma]$  are flagged as outliers and then not included in the next step. The process starts for  $n=10$  and stops at  $n=3$ . This last  
252 quality control removes ~1% of the total original sampling (as expected from a gaussian distribution) of drifter data that clearly  
253 revealed anomalous temperature values.

254 Validation statistics are quantified in terms of mean bias and Root-Mean-Square Difference (RMSD) from matchup  
255 temperature differences (namely, SST minus drifter). Each statistical parameter is associated with a 95% confidence interval  
256 computed through a bootstrap procedure (Efron 1994).

257 In order to evaluate the DOISST performance with respect to the model, the same validation procedure has been applied to the  
258 modeled SST.

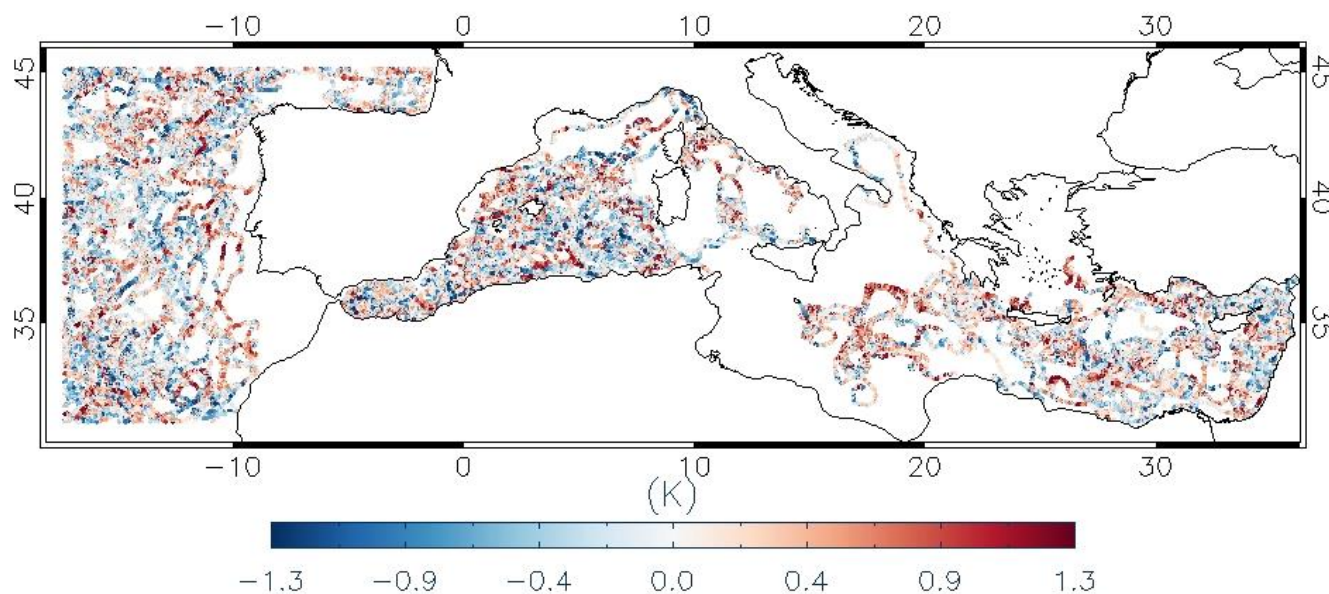
259



260 **4.2 Comparison with drifters**

261 **4.2.1 The mean diurnal cycle**

262 The spatial distribution of DOISST and drifter matchups over the 2019-2020 period, along with their pointwise bias (i.e.,  
 263 DOISST minus drifter measurement) shows a rather homogeneous coverage over the most of the CMEMS MED domain (Fig.  
 264 2), although some areas are characterized by quite low coverage, such as the North Adriatic Sea or North Aegean Sea. The  
 265 spatial distribution also evidences a positive tendency of the bias indicating that, on average, DOISSTs are warmer than  
 266 drifters' temperatures.



267  
 268 **Figure 2.** Spatial distribution of the matchup points along with their punctual bias (i.e., SST minus drifter data, K) over the  
 269 CMEMS Mediterranean domain from 2019/01/01 to 2020/12/31.

270  
 271  
 272 The DOISST product shows effectively an overall small positive mean bias of  $0.041 \pm 0.001$  K and a RMSD of  $0.412 \pm 0.001$   
 273 K (Table 2). A negative bias of  $-0.100 \pm 0.001$  K and slightly larger RMSD of  $0.467 \pm 0.001$  K characterize model SSTs.

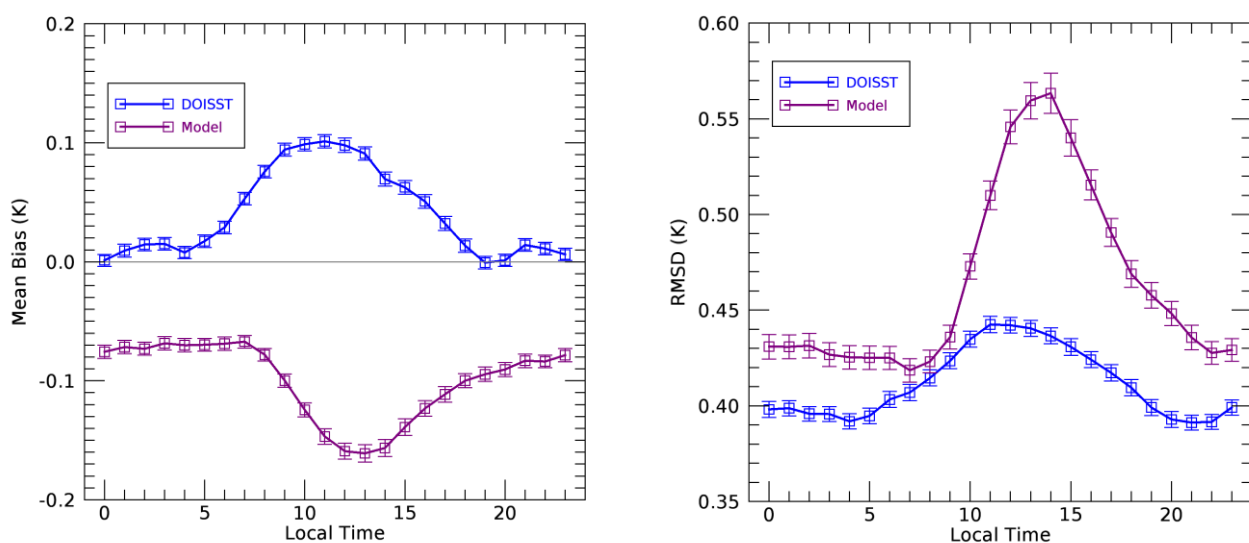
274

	Period	Mean bias (K)	RMSD (K)	Matchups
DOISST	2019-01-01 to 2020-12-31	$0.041 \pm 0.001$	$0.412 \pm 0.001$	548959
Model	2019-01-01 to 2020-12-31	$-0.100 \pm 0.001$	$0.467 \pm 0.001$	548959



275 **Table 2.** Summary statistics of DOISST and model outputs. Mean bias (K) and RMSD (K) are derived from temperature  
276 differences against drifters' data over the period 2019-2020.

277  
278 The hourly mean bias of DOISST and model shows similar but opposite behaviour (Fig. 3, and Table 3). In both cases, the  
279 bias clearly exhibits a diurnal oscillation during the 24 hours but, while the bias of DOISST increases positively during the  
280 central diurnal warming hours, the one of the model increases negatively. The DOISST mean bias is practically null between  
281 17:00 to 06:00 local time, ranging between -0.001 and 0.03 K, and highest ( $\sim 0.1$  K) between 10:00 and 13:00 local time. The  
282 bias of the model oscillates around  $\sim -0.07$  K between 23:00 and 07:00 local time. Then, it increases (in absolute value) reaching  
283 the peak of  $\sim -0.16$  K between 11:00 and 14:00 and decreases successively. Similar results are obtained for the RMSD, which  
284 increases with diurnal warming (Fig. 3, Table 3). However, the RMSD of DOISST is less impacted by diurnal variations,  
285 characterized by an amplitude of  $\sim 0.04$  K against  $\sim 0.14$  K of the model.



286 **Figure 3.** Mean bias (K) and RMSD (K) relative to MED DOISST (blue line) and model (purple line) based on the differences  
287 against drifters' data. Mean bias and RMSD are given as hourly mean over the period 2019-2020.



Hour (local time)	Mean BIAS (K) (DOISST)	RMSD (K) (DOISST)	BUOY-AVAIL	Mean BIAS (K) (Model)	RMSD (K) (Model)
HH: 00	0.001 ± 0.005	0.398 ± 0.004	22807	-0.076 ± 0.006	0.431 ± 0.006
HH: 01	0.009 ± 0.005	0.399 ± 0.004	23004	-0.072 ± 0.006	0.431 ± 0.006
HH: 02	0.014 ± 0.005	0.396 ± 0.004	22798	-0.073 ± 0.005	0.431 ± 0.006
HH: 03	0.015 ± 0.005	0.396 ± 0.004	23078	-0.068 ± 0.006	0.427 ± 0.006
HH: 04	0.008 ± 0.005	0.392 ± 0.004	22857	-0.070 ± 0.005	0.425 ± 0.006
HH: 05	0.017 ± 0.005	0.395 ± 0.004	22806	-0.070 ± 0.005	0.425 ± 0.006
HH: 06	0.029 ± 0.005	0.403 ± 0.004	22819	-0.069 ± 0.006	0.425 ± 0.006
HH: 07	0.053 ± 0.005	0.407 ± 0.004	23379	-0.067 ± 0.005	0.419 ± 0.006
HH: 08	0.076 ± 0.005	0.415 ± 0.004	23501	-0.078 ± 0.006	0.423 ± 0.006
HH: 09	0.094 ± 0.005	0.423 ± 0.004	23481	-0.100 ± 0.006	0.436 ± 0.006
HH: 10	0.099 ± 0.006	0.435 ± 0.004	23270	-0.125 ± 0.006	0.473 ± 0.007
HH: 11	0.101 ± 0.006	0.442 ± 0.004	23311	-0.147 ± 0.006	0.510 ± 0.007
HH: 12	0.098 ± 0.006	0.442 ± 0.004	23129	-0.159 ± 0.007	0.546 ± 0.009
HH: 13	0.091 ± 0.006	0.440 ± 0.005	22836	-0.161 ± 0.007	0.560 ± 0.009
HH: 14	0.070 ± 0.006	0.436 ± 0.004	22673	-0.157 ± 0.007	0.563 ± 0.011
HH: 15	0.062 ± 0.006	0.431 ± 0.004	22418	-0.139 ± 0.007	0.540 ± 0.009
HH: 16	0.051 ± 0.006	0.424 ± 0.004	22368	-0.123 ± 0.007	0.515 ± 0.008
HH: 17	0.032 ± 0.006	0.417 ± 0.004	22019	-0.111 ± 0.006	0.491 ± 0.007
HH: 18	0.014 ± 0.006	0.410 ± 0.004	21916	-0.100 ± 0.006	0.469 ± 0.007
HH: 19	-0.001 ± 0.005	0.399 ± 0.004	22117	-0.095 ± 0.006	0.458 ± 0.007
HH: 20	0.001 ± 0.005	0.393 ± 0.004	22458	-0.090 ± 0.006	0.448 ± 0.006
HH: 21	0.014 ± 0.005	0.391 ± 0.004	23229	-0.083 ± 0.005	0.436 ± 0.006
HH: 22	0.011 ± 0.005	0.392 ± 0.004	23272	-0.084 ± 0.006	0.428 ± 0.006
HH: 23	0.006 ± 0.005	0.399 ± 0.004	23413	-0.078 ± 0.006	0.429 ± 0.006

288

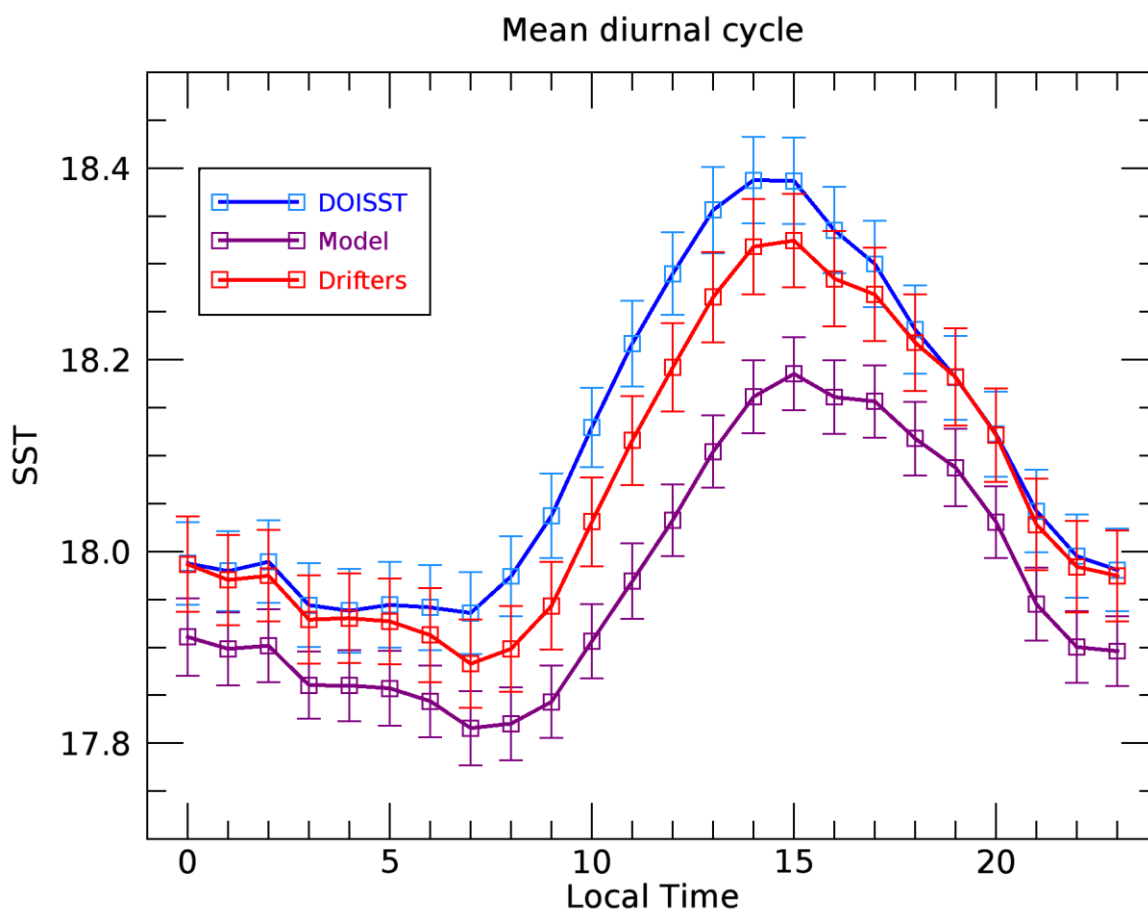
289 **Table 3.** Summary statistics of MED DOISST and model products based on the differences against drifters' data over the  
 290 matchup points. Mean bias (K), RMSD (K) and number of matchups are given as hourly mean over the period 2019-2020.

291

292 The mean diurnal cycle of DOISST (namely, the 24-hour mean SSTs estimated over the matchup dataset) is in very good  
 293 agreement, within the error confidence interval, with the SST cycle reconstructed from drifters (Fig. 4). The two diurnal cycles  
 294 are practically coincident between 17:00 and 06:00, while they are biased by ~0.1 K between sunrise and 16:00, coherently  
 295 with the DOISST bias oscillation (Fig. 3). This bias could be related to skin SST getting warmer faster than 20 cm temperature.  
 296 The diurnal cycle of model SST maintains always below that of in situ temperatures, evidencing larger differences during the  
 297 central diurnal warming hours (Fig. 4). However, apart from the biases likely induced by the different depths, the SST



298 amplitude as estimated from the DOISST and the model is  $\sim 2.3\%$  larger and  $\sim 16\%$  smaller than that of drifters, respectively,  
299 suggesting that the model tends to underestimate diurnal variations.

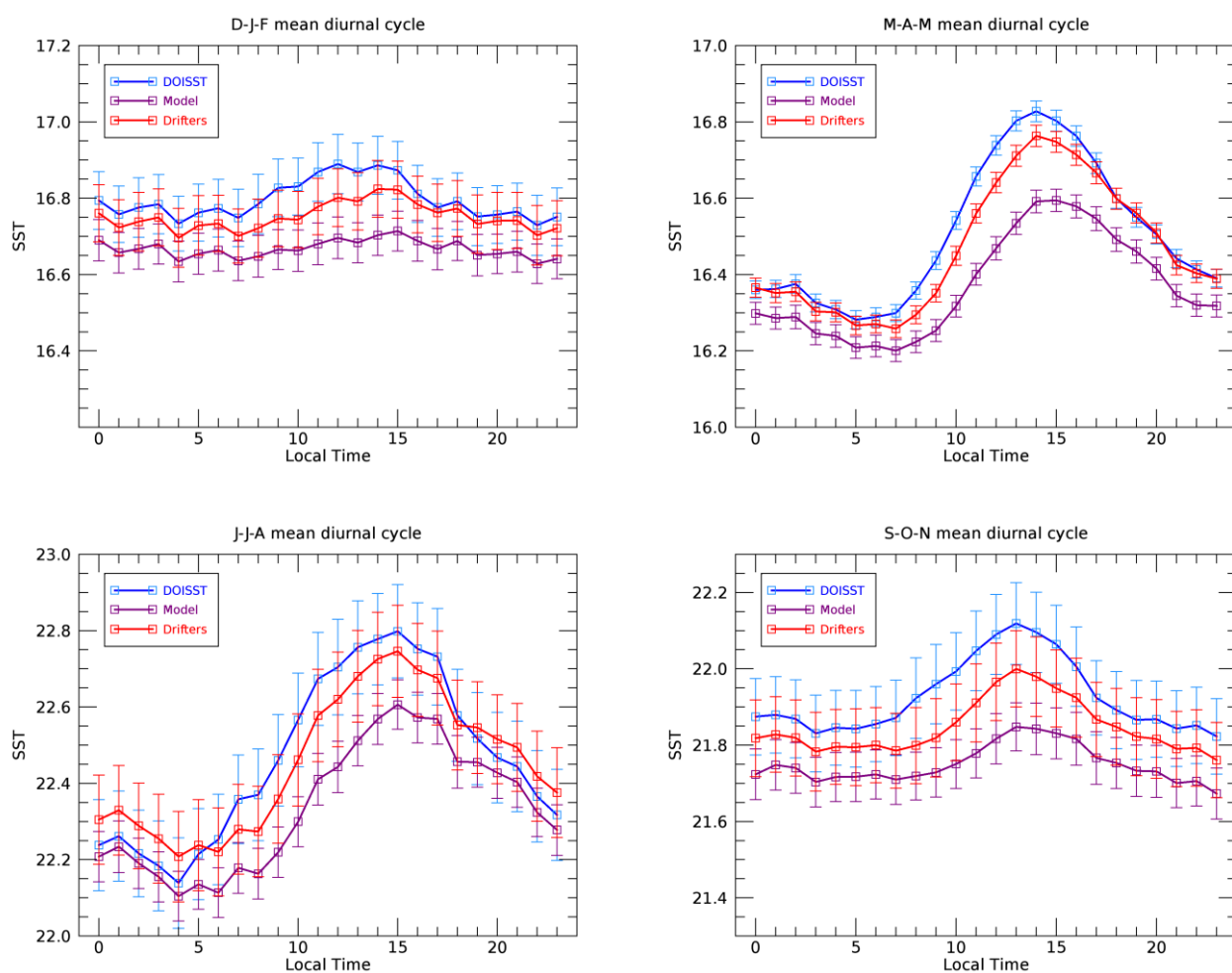


300  
301 **Figure 4.** Mean diurnal cycle for MED DOISST (blue line), model (purple line) and drifters (red line) computed over the  
302 matchups from 2019 to 2020.  
303

304 A delay of  $\sim 1$  hour of the model with respect to DOISST and in situ on the onset of diurnal warming and in reaching the  
305 maximum is also evident. This delay could be explained as the physical result of delayed solar heating of the skin layer sensed  
306 by the satellite and of the first model layer. This may also be a consequence of the different packaging of the SEVIRI and  
307 model SST data into the hourly files: model hourly SST fields are centered at half of every hour (e.g., 12:30), while SEVIRI  
308 L3C at the beginning of each hour (e.g., 12:00) and obtained from collating data within one hour (from 11.30 to 12:29).



309 The capability of DOISST to capture and realistically reproduce diurnal variability is further investigated by analysing the  
310 seasonally averaged SST diurnal cycle (Fig. 5), computed as for the mean diurnal cycle (by using the matchup dataset) but  
311 over seasons: winter (December to February, D-J-F), spring (March to May, M-A-M), summer (June to August, J-J-A) and  
312 autumn (September to November, S-O-N). The effect of warming in the diurnal SST excursion is clearly more pronounced  
313 during spring and summer than winter and autumn, and reconstructed well in DOISST. During the warmer seasons, the  
314 DOISST shows the lower biases (Table 4), estimated in  $0.036 \pm 0.001$  K (spring) and  $0.012 \pm 0.003$  K (summer). Conversely,  
315 the model reaches its higher biases, namely  $-0.101 \pm 0.001$  K (spring) and  $-0.117 \pm 0.003$  K (summer). The good agreement  
316 between DOISST and drifters during winter and autumn (Table 4) reveals that the hourly DOISST fields are reconstructed  
317 accurately also under cloudy conditions, which are more frequent during these seasons (Kotsias and Lolis, 2018).



318 **Figure 5.** Seasonal mean diurnal cycle over the period 2019-2020 for MED DOISST (blue line), model (purple line) in situ  
319 (red line).  
320



321

	<b>Period</b>	<b>Mean bias (K)</b>	<b>RMSD (K)</b>	<b>Matchups</b>
D-J-F	DOISST	$0.045 \pm 0.003$	$0.428 \pm 0.002$	90247
	Model	$-0.084 \pm 0.004$	$0.563 \pm 0.003$	
M-A-M	DOISST	$0.036 \pm 0.001$	$0.383 \pm 0.001$	308448
	Model	$-0.101 \pm 0.001$	$0.389 \pm 0.002$	
J-J-A	DOISST	$0.012 \pm 0.003$	$0.483 \pm 0.002$	74107
	Model	$-0.117 \pm 0.003$	$0.486 \pm 0.004$	
S-O-N	DOISST	$0.079 \pm 0.003$	$0.429 \pm 0.002$	76157
	Model	$-0.098 \pm 0.004$	$0.590 \pm 0.004$	

322 **Table 4.** Summary statistics of DOISST and model outputs. Mean bias (K) and RMSD (K) are derived from temperature  
 323 differences against drifters' data during winter (D-J-F), spring (M-A-M), summer (J-J-A) and autumn (S-O-N) over the period  
 324 2019-2020.

325  
 326  
 327  
 328

The capability of DOISST to reproduce diurnal warming events is analysed in the following section.

#### 329 4.2.2 Diurnal warming events

330 Diurnal warming (DW) can be defined as the (positive) difference between the SST at a given time of the day and the  
 331 foundation SST (see e.g. Minnett et al., 2019), i.e. the water temperature at a depth such that the daily variability induced by  
 332 the solar irradiance is negligible. In many cases, the foundation SST coincides with the night minimum SST, namely the  
 333 temperature that is recorded just before sunrise.

334 The capability of DOISST to describe diurnal warming events is analysed here in comparison with SEVIRI L3C, model and  
 335 drifter data. The evaluation is carried out by computing daily DWAs from drifters and building a matchup dataset of DWAs  
 336 as estimated from DOISST, SEVIRI L3C and model data. The inclusion of SEVIRI data is aimed at evaluating the impact of  
 337 optimal interpolation on the input SEVIRI SSTs. The diurnal warming amplitude (DWA) is estimated here as a difference  
 338 between the maximum occurred during daytime (10:00-18:00 local time) and the minimum during nighttime (00:00-06:00  
 339 local time) (see also Takaya et al., 2010; While et al., 2017).

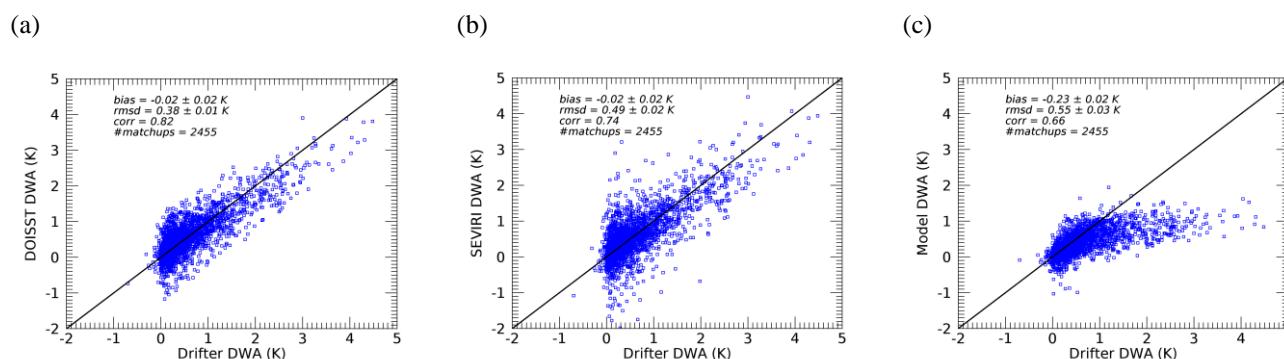
340 The scatter plots of DOISST, SEVIRI and model vs in situ-measured DWA have been computed for the years 2019-2020 (Fig.  
 341 6) and organized during spring-summer and winter-autumn seasons (Fig. 7). This choice is aimed at comparing the behaviour  
 342 of the three products as a function of the seasons, since larger DWA intensities are expected in the spring-summer period.



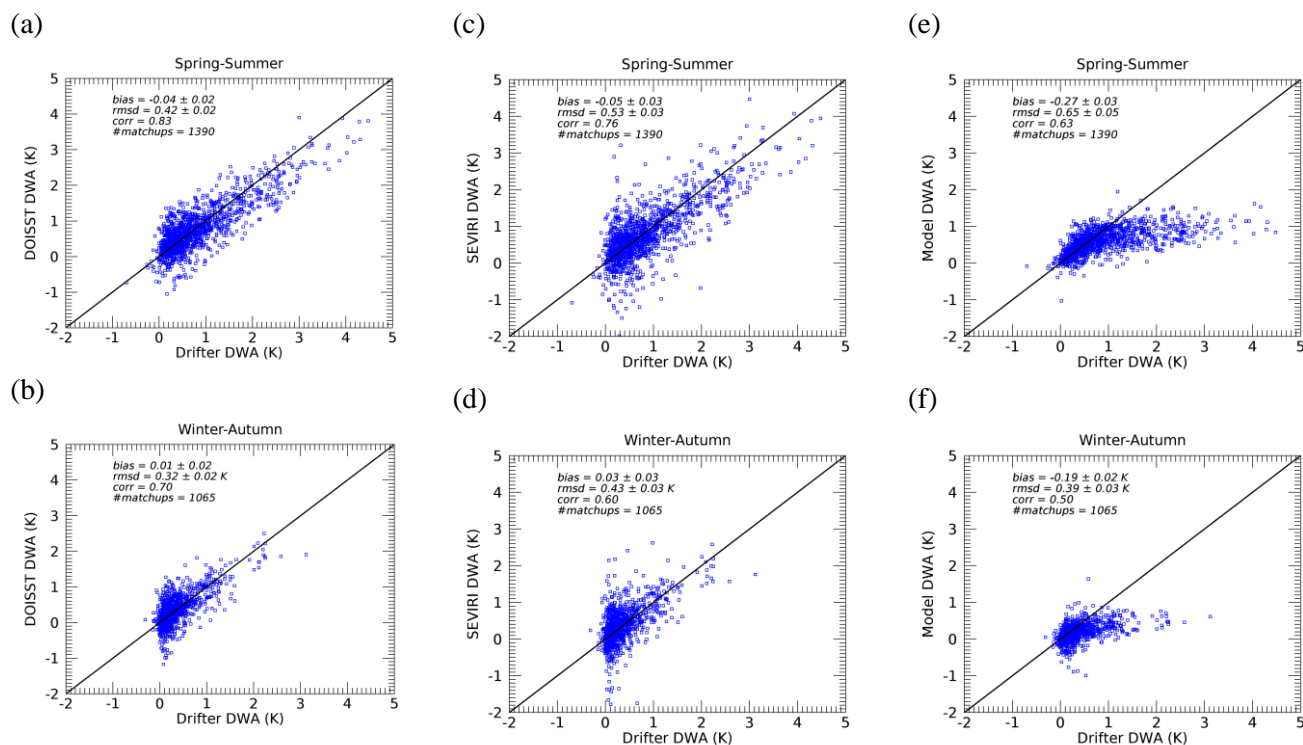


343 Overall, there is a good agreement between DOISST and drifter DWAs (Fig. 6a) as confirmed by an almost null mean bias (-  
344 0.02 K), low RMSD (0.38 K) and high correlation coefficient (0.82). The largest DW amplitudes reach values as high as 4 K  
345 in both DOISST and drifter data. SEVIRI (Fig. 6b) shows the same bias (-0.02 K) of DOISST in reconstructing DWAs but  
346 higher RMSD (0.49 K) and lower correlation (0.74). It is relevant to note that the spread of SEVIRI DWAs around the line of  
347 perfect agreement is reduced in DOISST, which coherently has a lower RMSD. The model (Fig. 6c) clearly underestimates  
348 diurnal amplitudes larger than 1 K, and it is characterized by the highest mean bias (-0.23 K) and RMSD (0.66 K), and lowest  
349 correlation coefficient (0.66).

350 The majority of DWA events lie between 0-1 K all over the year, but higher values are effectively reached during spring and  
351 summer (Fig. 7). During these seasons, it appears more evident the capability of DOISST to better describe DWAs larger than  
352 1 K (mean bias = -0.04 K; RMSD = 0.42 K; corr. = 0.83) compared to SEVIRI (mean bias = -0.05 K; RMSD = 0.53 K; corr.  
353 = 0.76) and especially to the model (mean bias = -0.27 K; RMSD = 0.65 K; corr. = 0.63). A similar behaviour is obtained  
354 during winter and autumn when DWA events exceeding 1 K are also observed, and such intense amplitudes are not found in  
355 the model-derived DWAs. Additionally, the good agreement between DOISST and drifters still confirms that interpolated data  
356 do not suffer from the increased cloud cover during winter and autumn periods.



357  
358 **Figure 6.** DWA scatter plots for (a) DOISST, (b) SEVIRI L3C and (c) model vs drifters over the period 2019-2020.  
359



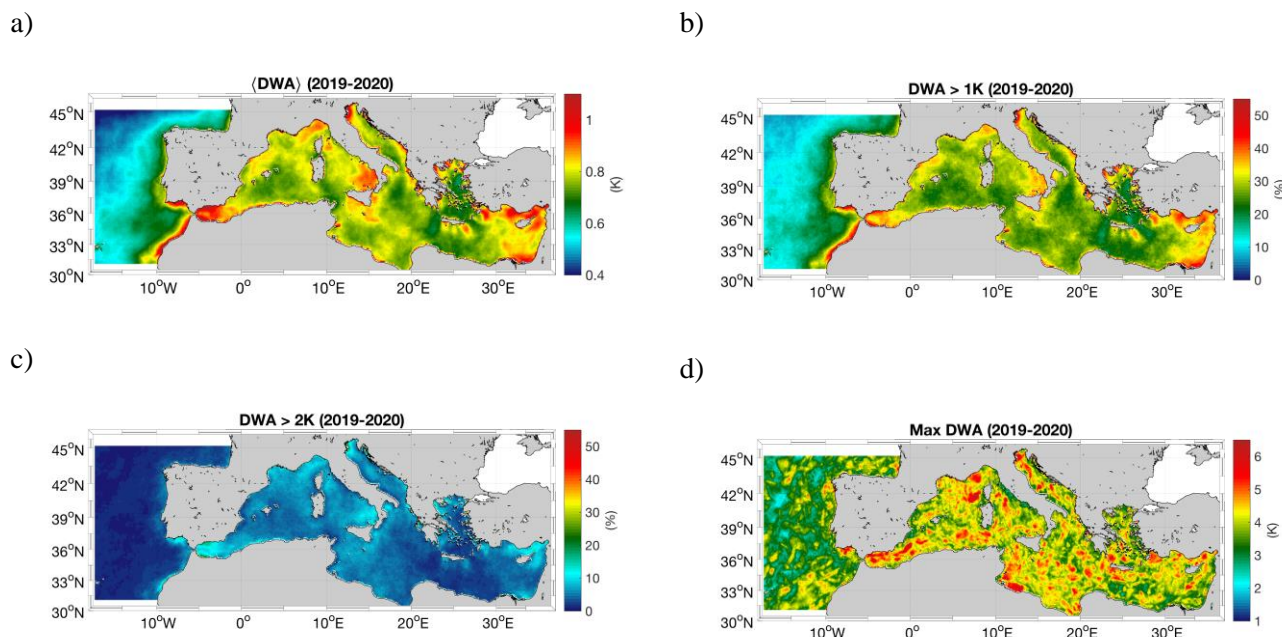
360 **Figure 7.** DWA scatter plots for DOISST (a,b), SEVIRI L3C (c,d) and model (e,f) vs drifters during Spring (M-A-M) and  
 361 Summer (J-J-A), and Winter (D-J-F) - Autumn (S-O-N), over the period 2019-2020.  
 362

363 Having demonstrated the reliability of DOISST in the DWA estimate, we analyze its capability to reproduce the typical spatial  
 364 variability and intensity of DW events in the Mediterranean Sea, a basin characterized by a frequent occurrence of intense DW  
 365 events (Böhm et al., 1991; Buongiorno Nardelli et al., 2005; Gentemann et al., 2008; Merchant et al., 2008). In our investigation  
 366 area, the 2019-2020 mean DWA ranges from a minimum of 0.4 K in the Atlantic ocean box off the Strait of Gibraltar, to a  
 367 maximum of 1.2 K in several regions of the Mediterranean Sea (Fig. 8a) where individual diurnal warming events exceeding  
 368 1 or even more than 2 K are quite frequent (Minnet et al. 2019; Marullo et al. 2016; Marullo et al 2014; see in particular Fig.  
 369 3 in Minnet et al., 2019]. The largest DWA were observed in the Levantine Basin, in the North Adriatic Sea and in  
 370 correspondence with the Alboran Gyre. Less intense, though still remarkable, mean DWA patches reaching 0.9 K are found  
 371 around the southern tip of the Italian Peninsula as well as in the coastal Ligurian Sea. In the same areas, it is found that the  
 372 frequency of DW events larger than 1 K and 2 K can reach up to 55% and 10% of the analyzed time series, respectively  
 373 (bearing in mind that our time series is given by the total number of days in 2019 and 2020) (Fig. 8b-c).

374

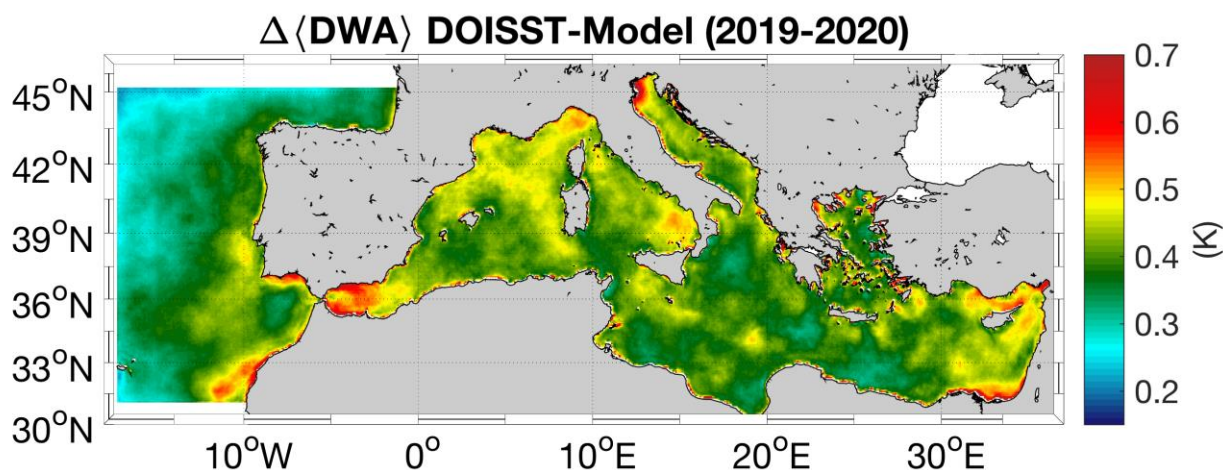


375 The magnitude of the maximum SST diurnal oscillation is also investigated. The spatial distribution of the maximum DWA  
376 observed through 2019-2020 in the Mediterranean Sea (6°W to 36°E and 30°N to 46°N) (Fig. 8d) shows that the largest  
377 amplitudes reach and exceed 3 K in 98% of the basin and local DWA patches exceeding 6 K are also ubiquitous, confirming  
378 that the Mediterranean is one of the areas with the largest DWs of the global ocean (Minnet et al. 2019, and references therein).



379  
380 **Figure 8.** a) Mean diurnal warming amplitude (DWA) derived from DOISST; b) Percentage (over the total number of days in  
381 the 2019-2020 period) of DOISST DWA larger than 1 K; c) Percentage of DOISST DWA larger than 2 K; d) Maximum  
382 observed DOISST DWA. All the maps refer to the 2019-2020 period.

383  
384 When compared to the model, DOISST exhibits mean DWAs with larger intensity than model outputs in all the locations of  
385 the study area (Fig. 9). The  $\Delta$ DWA, defined as  $DWA_{DOISST}$  minus  $DWA_{Model}$ , is always larger than 0.2 K and locally reaches  
386 extreme values of  $\sim 1$  K. The extent of the  $\Delta$ DWA generally increases in areas where the DOISST mean DWA is larger, such  
387 as in the Alboran Sea, Ligurian Sea, Levantine Basin and Southern Tyrrhenian, suggesting a tendency of the model to  
388 underestimate the largest DW events.



389 **Figure 9.** Mean amplitude of the SST DW. Differences between the mean DWA seen by the DOISST product and the  
390 model outputs (first layer).  
391  
392

### 393 **5 Data availability**

394 The Mediterranean diurnal optimal interpolated SST product is distributed as part of the CMEMS catalogue, and identified as  
395 SST\_MED\_PHY\_SUBSKIN\_L4\_NRT\_010\_036 (CMEMS product reference) and cmems\_obs-sst\_med\_phy-  
396 sst\_nrt\_diurnal-oi-0.0625deg\_PT1H-m (CMEMS dataset reference) ([https://resources.marine.copernicus.eu/product-  
397 detail/SST\\_MED\\_PHY\\_SUBSKIN\\_L4\\_NRT\\_010\\_036/INFORMATION](https://resources.marine.copernicus.eu/product-detail/SST_MED_PHY_SUBSKIN_L4_NRT_010_036/INFORMATION), last access: 03 November 2021,  
398 [https://doi.org/10.25423/CMCC/SST\\_MED\\_PHY\\_SUBSKIN\\_L4\\_NRT\\_010\\_036](https://doi.org/10.25423/CMCC/SST_MED_PHY_SUBSKIN_L4_NRT_010_036); Pisano et al, 2021). Access to the product  
399 is granted after free registration as a user of CMEMS at <https://resources.marine.copernicus.eu/registration-form> (last access:  
400 03 November 2021). Once registered, users can download the product through a number of different tools and services,  
401 including the web portal Subsetter, Direct-GetFile (DGF) and FTP. A Product User Manual (PUM) and Quality Information  
402 Document (QUID) are also available as part of the CMEMS documentation ([https://resources.marine.copernicus.eu/product-  
403 detail/SST\\_MED\\_PHY\\_SUBSKIN\\_L4\\_NRT\\_010\\_036/DOCUMENTATION](https://resources.marine.copernicus.eu/product-detail/SST_MED_PHY_SUBSKIN_L4_NRT_010_036/DOCUMENTATION), last access: 03 November 2021). Eventual  
404 updates of the product will be reflected in these documents. The basic characteristics of the DOISST product are summarized  
405 in Table 1. The reduced subset used here for validation and review purposes is openly available at  
406 <https://doi.org/10.5281/zenodo.5807729> (Pisano, 2021).



407

## 408 **6 Summary and conclusions**

409 A new operational Mediterranean diurnally varying SST product has been released (May 2021) within the Copernicus Marine  
410 Environment Monitoring Service (CMEMS). This dataset provides optimally interpolated (L4) hourly mean maps of sub-skin  
411 SST over the Mediterranean Sea at 1/16° horizontal resolution, covering the period from 1<sup>st</sup> January 2019 to near real time (1  
412 day before real time) (Pisano et al., 2021). The diurnal optimal interpolated SST (DOISST) product is obtained from a blending  
413 of hourly satellite (SEVIRI) data and model outputs via optimal interpolation, where the former are used as the observation  
414 source and the latter as background. This method has been firstly proposed by Marullo et al. (2014), validated over one year  
415 (2013) in Marullo et al. (2016), and implemented here operationally. The validation of the operational product was also  
416 extended over two years (2019-2020).

417 DOISST proved to be rather accurate when compared to drifter measurements, and correctly reproduced the diurnal variability  
418 in the Mediterranean Sea. The accuracy of DOISST results in an overall, almost null, mean bias of ~0.04 K and RMSD of  
419 ~0.41 K (Table 2). This product is also more accurate than the input model, which shows a mean bias of ~-0.1 K and RMSD  
420 of ~0.47 K. A warm (positive) and cold (negative) bias characterizes the DOISST and the model, respectively, also during  
421 seasons (Fig. 5). These opposite biases are likely related to the different nature of the SST provided by DOISST, model and  
422 drifter data, i.e. sub-skin (upper first millimeters from the surface), averaged 1 m depth and 20 cm depth, respectively, and  
423 then consistent with the physical consequence of a reduction of the temperature with depth due to the vertical transfer heat  
424 process. The DOISST RMSD generally keeps lower values compared to the model, ranging from a minimum of ~0.40 K (vs  
425 ~0.42 K for the model) to a maximum of ~0.44 K (vs ~0.56 K for the model).

426 Compared to its native version (Marullo et al., 2016), the DOISST product maintains the same RMSD (estimated in 0.42 K)  
427 but displays a lower mean bias (estimated as -0.10 K). The reduced bias could be ascribed to the fact that valid SEVIRI SST  
428 values are always interpolated in DOISST, while they are left unchanged in the original method. The DOISST bias is also  
429 lower than that of the OSTIA diurnal product, which produces gap-free hourly mean fields of skin SST for the global ocean,  
430 and has been found to underestimate the diurnal range of skin SST by 0.1-0.3 °C (While et al., 2017).

431 The analysis of the SST diurnal cycle as estimated from both DOISST, model and drifter data shows that the diurnal oscillation  
432 in SST is well reconstructed by the DOISST while the model tends to underestimate this amplitude mainly during the central  
433 warming hours (Fig. 4), and during spring and summer (Fig. 5). Specifically, DOISST overestimates the mean diurnal  
434 amplitude by ~2.3% compared to that of drifters, while the model underestimates it by ~16%. This is particularly evident in  
435 the analysis of diurnal warming (DW) events, where diurnal warming amplitudes (DWAs) as estimated by DOISST, model  
436 and SEVIRI data are compared vs drifter-derived DWAs. This analysis shows that amplitudes exceeding 1 K as measured by



437 drifters are well reconstructed by DOISST (Fig. 6a) with a mean bias of  $\sim -0.02$  K while model SSTs show significantly lower  
438 values, with a mean bias of  $\sim -0.23$  K (Fig. 6c). The underestimation of the diurnal warming amplitude (DWA) by the model  
439 could be related to several factors, such as that the vertical resolution does not resolve the vertical temperature profile within  
440 the warm layer, the physics and atmospheric forcing implemented in the model, and/or the assimilation of the foundation SST  
441 fields used for the correction of surface heat flux.

442 The comparison with reconstructed SEVIRI DWAs (Fig. 6b) demonstrates that optimal interpolation does not change the  
443 SEVIRI bias, which is practically null for both SEVIRI and DOISST ( $\sim -0.02$  K), while it reduces the SEVIRI RMSD, from  
444  $\sim 0.49$  K (SEVIRI) to  $\sim 0.38$  K (DOISST). The seasonal analysis also reveals that DOISST is not impacted by the different  
445 environmental conditions in the Mediterranean Sea, in particular from the much frequent cloudiness during winter and autumn  
446 periods.

447 Overall, the DOISST product is able to accurately reconstruct the SST diurnal cycle, including diurnal warming events, for the  
448 Mediterranean Sea and can thus represent a valuable dataset to improve the study of those processes that require sub-daily  
449 frequency.

450  
451

## 452 **Financial Support**

453 This work has been carried out within the Copernicus Marine Environment Monitoring Service (CMEMS) Sea Surface  
454 Temperature Thematic Assembly Centre (SST TAC), contract n° 78-CMEMS-TAC-SST. This contract is funded by Mercator  
455 Océan International as part of its delegation agreement with the European Union, represented by the European Commission,  
456 to set-up and manage CMEMS.

457

## 458 **References**

459 Bernie, D. J., Guilyardi, E., Madec, G., Slingo, J. M., Woolnough, S. J., and Cole, J. (2008). Impact of resolving the diurnal  
460 cycle in an ocean–atmosphere GCM. Part 2: A diurnally coupled CGCM. *Climate dynamics*, 31(7-8), 909-925.

461 Böhm, E., Marullo, S., and Santoleri, R. (1991). AVHRR visible-IR detection of diurnal warming events in the western  
462 Mediterranean Sea. *International Journal of Remote Sensing*, 12(4), 695-701.

463 Bowen, M. M., Emery, W. J., Wilkin, J. L., Tildesley, P. C., Barton, I. J., and Knewton, R. (2002). Extracting multiyear  
464 surface currents from sequential thermal imagery using the maximum cross-correlation technique. *Journal of Atmospheric and*  
465 *Oceanic Technology*, 19(10), 1665-1676.



- 466 Bretherton, F. P., Davis, R. E., and Fandry, C. B. (1976). A technique for objective analysis and design of oceanographic  
467 experiments applied to MODE-73. In *Deep Sea Research and Oceanographic Abstracts* (Vol. 23, No. 7, pp. 559-582). Elsevier.
- 468 Buongiorno Nardelli, B.; Marullo, S.; Santoleri, R. (2005). Diurnal Variations in AVHRR SST Fields: A Strategy for  
469 Removing Warm Layer Effects from Daily Images. *Remote Sens. Environ.*, 95 (1), 47–56.  
470 <https://doi.org/10.1016/j.rse.2004.12.005>.
- 471 Buongiorno Nardelli, B., Tronconi, C., Pisano, A., and Santoleri, R. (2013). High and Ultra-High resolution processing of  
472 satellite Sea Surface Temperature data over Southern European Seas in the framework of MyOcean project. *Remote Sensing  
473 of Environment*, 129, 1-16.
- 474 Chen, S. S., and Houze Jr, R. A. (1997). Diurnal variation and life-cycle of deep convective systems over the tropical Pacific  
475 warm pool. *Quarterly Journal of the Royal Meteorological Society*, 123(538), 357-388.
- 476 Clayson, C. A., and Bogdanoff, A. S. (2013). The effect of diurnal sea surface temperature warming on climatological air–sea  
477 fluxes. *Journal of Climate*, 26(8), 2546-2556.
- 478 Clementi, E., Oddo, P., Drudi, M., Pinardi, N., Korres, G., and Grandi A. (2017). Coupling hydrodynamic and wave models:  
479 first step and sensitivity experiments in the Mediterranean Sea. *Ocean Dynamics*. doi: [https://doi.org/10.1007/s10236-017-  
480 1087-7](https://doi.org/10.1007/s10236-017-1087-7).
- 481 Clementi, E., Aydogdu, A., Goglio, A. C., Pistoia, J., Escudier, R., Drudi, M., Grandi, A., Mariani, A., Lyubartsev, V., Lecci,  
482 R., Cretí, S., Coppini, G., Masina, S., & Pinardi, N. (2021). Mediterranean Sea Physical Analysis and Forecast (CMEMS  
483 MED-Currents, EAS6 system) (Version 1) [\[Data set\]](#). Copernicus Monitoring Environment Marine Service (CMEMS).
- 484 Deser, C., Alexander, M. A., Xie, S. P., and Phillips, A. S. (2010). Sea surface temperature variability: Patterns and  
485 mechanisms. *Annual review of marine science*, 2, 115-143.
- 486 Dobricic, S., and Pinardi, N. (2008). An oceanographic three-dimensional variational data assimilation scheme. *Ocean  
487 modelling*, 22(3-4), 89-105.
- 488 Efron, B.; Tibshirani, R.J. *An Introduction to the Bootstrap*; CRC Press: Boca Raton, FL, USA, 1994.
- 489 Fiedler, E. K., McLaren, A., Banzon, V., Brasnett, B., Ishizaki, S., Kennedy, J., ... and Donlon, C. (2019). Intercomparison of  
490 long-term sea surface temperature analyses using the GHRSSST Multi-Product Ensemble (GMPE) system. *Remote sensing of  
491 environment*, 222, 18-33.



- 492 Gentemann, C. L., Minnett, P. J., Le Borgne, P., and Merchant, C. J. (2008). Multi-satellite measurements of large diurnal  
493 warming events. *Geophysical Research Letters*, 35, L22602. <http://dx.doi.org/10.1029/2008GL035730>.
- 494 Gentemann, C. L., and Minnett, P. J. (2008). Radiometric measurements of ocean surface thermal variability. *Journal of*  
495 *Geophysical Research: Oceans*, 113(C8).
- 496 Good, S. A., Corlett, G. K., Remedios, J. J., Noyes, E. J., and Llewellyn-Jones, D. T. (2007). The global trend in sea surface  
497 temperature from 20 years of advanced very high resolution radiometer data. *Journal of climate*, 20(7), 1255-1264.
- 498 Good, S., Fiedler, E., Mao, C., Martin, M.J., Maycock, A., Reid, R., Roberts-Jones, J., Searle, T., Waters, J., While, J., and  
499 Worsfold, M. (2020). The Current Configuration of the OSTIA System for Operational Production of Foundation Sea Surface  
500 Temperature and Ice Concentration Analyses. *Remote Sensing*, 12(720), doi:10.3390/rs12040720
- 501 Huang, B., Liu, C., Freeman, E., Graham, G., Smith, T., & Zhang, H. M. (2021). Assessment and Intercomparison of NOAA  
502 Daily Optimum Interpolation Sea Surface Temperature (DOISST) Version 2.1. *Journal of Climate*, 34(18), 7421-7441.
- 503 Kotsias, G., & Lolis, C. J. (2018). A study on the total cloud cover variability over the Mediterranean region during the period  
504 1979–2014 with the use of the ERA-Interim database. *Theoretical and Applied Climatology*, 134(1), 325-336.
- 505 Le Traon, P. Y., Reppucci, A., Alvarez Fanjul, E., Aouf, L., Behrens, A., Belmonte, M., ... and Zacharioudaki, A. (2019).  
506 From observation to information and users: The Copernicus Marine Service perspective. *Frontiers in Marine Science*, 6, 234.
- 507 Marullo, S., Minnett, P. J., Santoleri, R., and Tonani, M. (2016). The diurnal cycle of sea-surface temperature and estimation  
508 of the heat budget of the Mediterranean Sea. *Journal of Geophysical Research: Oceans*, 121(11), 8351-8367.
- 509 Marullo, S., Santoleri, R., Ciani, D., Le Borgne, P., Péré, S., Pinardi, N., Tonani, M., and Nardone, G. (2014). Combining  
510 model and geostationary satellite data to reconstruct hourly SST field over the Mediterranean Sea. *Remote sensing of*  
511 *environment*, 146, 11-23.
- 512 Merchant, C. J., Embury, O., Bulgin, C. E., Block, T., Corlett, G. K., Fiedler, E., ... and Donlon, C. (2019). Satellite-based  
513 time-series of sea-surface temperature since 1981 for climate applications. *Scientific data*, 6(1), 1-18.
- 514 Merchant, C. J., Filippiak, M. J., Le Borgne, P., Roquet, H., Autret, E., Piollé, J. F., & Lavender, S. (2008). Diurnal warm-layer  
515 events in the western Mediterranean and European shelf seas. *Geophysical Research Letters*, 35(4).
- 516 Minnett, P. J., Alvera-Azcárate, A., Chin, T. M., Corlett, G. K., Gentemann, C. L., Karagali, I., ... and Vazquez-Cuervo, J.  
517 (2019). Half a century of satellite remote sensing of sea-surface temperature. *Remote Sensing of Environment*, 233, 111366.





- 518 Oddo, P., Bonaduce, A., Pinardi, N., and Guarneri, A. (2014) Sensitivity of the Mediterranean sea level to atmospheric  
519 pressure and free surface elevation numerical formulation in NEMO. *Geosci. Model Dev.*, 7, 3001–3015.
- 520 Oddo, P., Adani, M., Pinardi, N., Fratianni, C., Tonani, M., and Pettenuzzo, D. (2009). A Nested Atlantic-Mediterranean Sea  
521 General Circulation Model for Operational Forecasting. *Ocean Sci. Discuss.*, 6, 1093-1127.
- 522 Oliver, E. C., Benthuisen, J. A., Darmaraki, S., Donat, M. G., Hobday, A. J., Holbrook, N. J., ... and Sen Gupta, A. (2021).  
523 Marine heatwaves. *Annual Review of Marine Science*, 13, 313-342.
- 524 Pinardi, N., Allen, I., De Mey, P., Korres, G., Lascaratos, A., Le Traon, P.Y., Maillard, C., Manzella G., and Tziavos, C.  
525 (2003). The Mediterranean ocean Forecasting System: first phase of implementation (1998-2001). *Ann. Geophys.*, 21, 1, 3-  
526 20.
- 527 Pisano, A., Marullo, S., Artale, V., Falcini, F., Yang, C., Leonelli, F. E., ... and Buongiorno Nardelli, B. (2020). New evidence  
528 of mediterranean climate change and variability from sea surface temperature observations. *Remote Sensing*, 12(1), 132.
- 529 Pisano, A., Buongiorno Nardelli, B., Marullo, S., Rosalia, S., Tronconi, C., & Ciani, D. (2021). Mediterranean Sea - High  
530 Resolution Diurnal Subskin Sea Surface Temperature Analysis (Version 1) [Data set]. Copernicus Marine Environment  
531 Monitoring Service (CMEMS). [https://doi.org/10.25423/CMCC/SST\\_MED\\_PHY\\_SUBSKIN\\_L4\\_NRT\\_010\\_036](https://doi.org/10.25423/CMCC/SST_MED_PHY_SUBSKIN_L4_NRT_010_036)
- 532 Pisano, Andrea. (2021). CNR Mediterranean Sea High Resolution Diurnal Subskin Sea Surface Temperature Analysis:  
533 Validation subset. <https://doi.org/10.5281/zenodo.5807729>
- 534 Reverdin, G., Boutin, J., Martin, N., Lourenço, A., Bouruet-Aubertot, P., Lavin, A., ... and Lazure, P. (2010). Temperature  
535 measurements from surface drifters. *Journal of Atmospheric and Oceanic Technology*, 27(8), 1403-1409.
- 536 Rio, M. H., and Santoleri, R. (2018). Improved global surface currents from the merging of altimetry and sea surface  
537 temperature data. *Remote sensing of Environment*, 216, 770-785.
- 538 Storto, A., and Oddo, P. (2019). Optimal assimilation of daytime SST retrievals from SEVIRI in a regional ocean prediction  
539 system. *Remote Sensing*, 11(23), 2776.
- 540 Takaya, Y., Bidlot, J. R., Beljaars, A. C., & Janssen, P. A. (2010). Refinements to a prognostic scheme of skin sea surface  
541 temperature. *Journal of Geophysical Research: Oceans*, 115(C6).
- 542 Yang, C., Leonelli, F. E., Marullo, S., Artale, V., Beggs, H., Nardelli, B. B., ... and Pisano, A. (2021). Sea Surface Temperature  
543 Intercomparison in the Framework of the Copernicus Climate Change Service (C3S). *Journal of Climate*, 34(13), 5257-5283.



544 Waters, J., Lea, D. J., Martin, M. J., Mirouze, I., Weaver, A., and While, J. (2015). Implementing a variational data assimilation  
545 system in an operational 1/4 degree global ocean model. Quarterly Journal of the Royal Meteorological Society, 141(687),  
546 333-349.

547 While, J., Mao, C., Martin, M. J., Roberts-Jones, J., Sykes, P. A., Good, S. A., and McLaren, A. J. (2017). An operational  
548 analysis system for the global diurnal cycle of sea surface temperature: implementation and validation. Quarterly Journal of  
549 the Royal Meteorological Society, 143(705), 1787-1803.

550

551

552